

Polarization of Light

PHY324, February 19 2023

Emre Alca 1005756193, Jace Alloway 1006940802

Abstract

Lore ipsum dolor sit amet, consectetur adipiscing elit. Ut purus elit, vestibulum ut, placerat ac, adipiscing vitae, felis. Curabitur dictum gravida mauris. Nam arcu libero, nonummy eget, consectetur id, vulputate a, magna. Donec vehicula augue eu neque. Pellentesque habitant morbi tristique senectus et netus et malesuada fames ac turpis egestas. Mauris ut leo. Cras viverra metus rhoncus sem. Nulla et lectus vestibulum urna fringilla ultrices. Phasellus eu tellus sit amet tortor gravida placerat. Integer sapien est, iaculis in, pretium quis, viverra ac, nunc. Praesent eget sem vel leo ultrices bibendum. Aenean faucibus. Morbi dolor nulla, malesuada eu, pulvinar at, mollis ac, nulla. Curabitur auctor semper nulla. Donec varius orci eget risus. Duis nibh mi, congue eu, accumsan eleifend, sagittis quis, diam. Duis eget orci sit amet orci dignissim rutrum.

Introduction

In introductory optics and electromagnetism, light polarization is the intrinsic property of electromagnetic waves which is given by the orientation of propagation. Generally, there are three types of light polarization: linear, circular, and elliptical. Most light is linearly polarized, and may be manually polarized by means of a polarizer, by reflection, scattering, or refraction through denser media.

Maxwell's equations predict the linear polarization of light as perpendicular electric and magnetic field components, which then are both perpendicular to the direction of the propagation. This allows various projections of these components on vertical and horizontal axes, hence polarizing the light. Any light passing through a polarizer is then polarized in the direction of the polarizer.

Today, polarizers are used in sunglasses, laser physics, photography, and other ranges of electromagnetic waves (radio, x-rays, gamma rays, etc).

Theory

In the absence of electric charge and current distributions, Maxwell's equations may be rearranged and re-substituted to obtain the wave equations for typical electric and magnetic field components:

$$\square^2 \mathbf{E}(\mathbf{r}, t) = 0, \quad \square^2 \mathbf{B}(\mathbf{r}, t) = 0, \quad (1)$$

where $\square^2 \equiv \nabla^2 - \frac{1}{c^2} \frac{\partial^2}{\partial t^2}$ is the D'Alembertian operator. Solving these equations by D'Alembert's method provides expressions for \mathbf{E} and \mathbf{B} as

$$\mathbf{E}(\mathbf{r}, t) = \operatorname{Re} \left\{ \mathcal{E}_0 \exp \left(i \frac{\omega}{c} (\mathbf{n} \cdot \mathbf{r} - ct) \right) \right\} \quad (2.1)$$

$$\mathbf{B}(\mathbf{r}, t) = \operatorname{Re} \left\{ \mathcal{B}_0 \exp \left(i \frac{\omega}{c} (\mathbf{n} \cdot \mathbf{r} - ct) \right) \right\}, \quad (2.2)$$

where \mathcal{E}_0 and \mathcal{B}_0 are the electric and magnetic wave directions, respectively, ω is the angular frequency of the wave, and \mathbf{n} the direction of propagation.

Then, (2.1) and (2.2) are related by Faraday's Law,

$$\nabla \times \mathbf{E} + \frac{\partial \mathbf{B}}{\partial t} = 0, \quad (3)$$

which yields the electro-magnetic wave relation

$$\operatorname{Re} \left\{ \left(i \frac{\omega}{c} \mathbf{n} \times \mathcal{E}_0 - i\omega \mathcal{B}_0 \exp \left(i \frac{\omega}{c} (\mathbf{n} \cdot \mathbf{r} - ct) \right) \right) \right\} = 0, \quad (4)$$

which is true for all space and time components.

Therefore $\mathcal{B}_0 = \frac{1}{c} \mathbf{n} \times \mathcal{E}_0$, resulting in perpendicular electric and magnetic field components of a light wave. Polarization is the effect of projecting these vector components of (4) onto a plane, reducing the light intensity and specifying a polarized direction.

This report focuses on two interesting effects of light polarization: Malus's law, and reflectance polarization in the form of Brewster's angle. Malus's

law models the effects of polarizers aligned in series to each other, and how the intensity of the light changes.

In its simplest form, Malus's law states that the intensity of light as it passes through two polarizers is proportional to $\cos^2 \theta$, where θ is the angle between the two polarizers. Suppose the polarizer is oriented in the \hat{y} direction, and let the transmission axis of this second polarizer be \hat{y}' . In this case, the components of the wave which pass through this second polarizer is

$$E_{x'} = E \sin \theta \quad E_{y'} = E \cos \theta \quad (5)$$

with the \hat{y}' component being transmitted only (since \hat{x}' is orthogonal to the transmission axis of the second polarizer). By definition, since intensity is proportional to the square of the electric field component, $I_0 \propto E^2$ (the intensity between the polarizers), thus the intensity of light transmitted by both of them is

$$I(\theta) = E^2 \cos^2 \theta = I_0 \cos^2 \theta \quad (6)$$

This expression is called Malus's Law. For this experiment, θ is known from our measurements, and $I(\theta)$ will be extrapolated using an optimization algorithm.

For two polarizers perpendicular to each other, then, it is expected and observed that the output intensity is indeed zero:

$$\begin{aligned} I(\pi/2) &= I_0 \cos^2(\pi/2) \\ &= 0. \end{aligned} \quad (7)$$

If a third polarizer is placed further along the \hat{z} axis such that its transmission axis is orthogonal to that of the first polarizer, some intensity does, interestingly enough, transmit through. The intensity that passes through this third polarizer can be found by applying Malus's law a second time in series. If the intensity of light passing through the first polarizer is I_1 , then the intensity through the analyzer is

$$I_1 = I_0 \cos^2 \varphi \quad (8)$$

where φ is the angle between the transmission axes of the polarizer and analyzer. Then $\theta + \varphi = \frac{\pi}{2}$. Applying Malus's law a second time,

$$I_2 = I_1 \cos^2 \left(\frac{\pi}{2} - \varphi \right) \quad (9.1)$$

$$= I_0 \cos^2(\varphi) \cos^2 \left(\frac{\pi}{2} - \varphi \right) \quad (9.2)$$

$$= \frac{I_0}{4} \sin^2(2\varphi) \quad (9.3)$$

A representation of this phenomenon is shown in Figure 1.

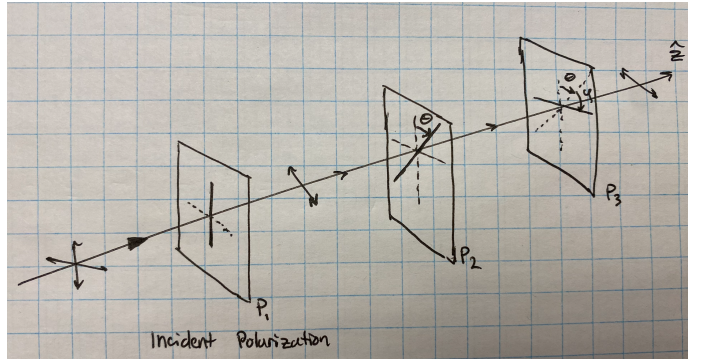


[Figure 1] The effect of three-polarizer polarization on an incident beam of vertically-polarized light.

In the same way, light can be polarized by means of reflection and transmission upon incidence on different types of media. For reflections on air-glass interfaces, the Fresnel equations provide expressions for the parallel and perpendicular reflectance coefficients r_{\parallel} and r_{\perp} :

$$r_{\perp} = \frac{n_1 \cos \theta_1 - n_2 \cos \theta_2}{n_1 \cos \theta_1 + n_2 \cos \theta_2} \quad (10.1)$$

$$r_{\parallel} = \frac{n_1 \cos \theta_2 - n_2 \cos \theta_1}{n_1 \cos \theta_2 + n_2 \cos \theta_1} \quad (10.2)$$

$$r_{\parallel}^2 + r_{\perp}^2 = 1. \quad (10.3)$$

In practice, these coefficients relate the reflected and transmission angles (θ_1 and θ_2 , respectively) with the refraction indices (n_1 and n_2), which are also related by Snell's law of refraction

$$\frac{\sin \theta_2}{\sin \theta_1} = \frac{n_1}{n_2}. \quad (11)$$

The angle at which the reflectance coefficient r_{\perp}^2 is zero is called Brewster's angle, and is given by $\tan \theta_p = \frac{n_2}{n_1}$. This yields a value of n_2 , and by equation (11), the transmission angle θ_2 can be determined, thus determining the transmission coefficient r_{\parallel}^2 , which is the amount of light transmitted upon polarization with the medium.

Experimentally, for vertically polarized light, θ_p can be determined by reading off from data from

where the reflected horizontally polarized intensity in terms of θ_1 is zero, and this determines Brewster's angle and hence the index of refraction of the medium n_2 . These processes are described in the methodology.

Methodology

The following experimental trials were performed in a dark room with minimal light. To begin, a small 10-volt laser beam was attached to the end of a long track with two polarizers in series with one another. At the end of the track, a laser-acquisition device was placed with a collimating slit in front of it to filter some of the light out to avoid oversaturating the detector. The detector gain level was set to '1', and one of the polarizers was linked to LabView. It was manually rotated 2π radians while LabView acquired the data. These measurements were repeated until the best, smoothest curve was measured. The apparatus is shown in Figure 2.

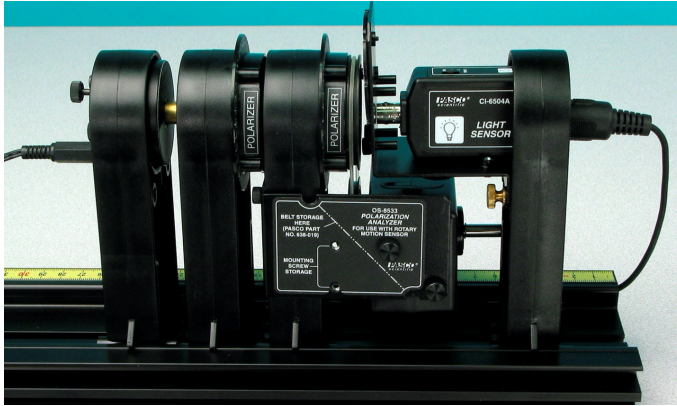


[Figure 2] Experimental setup and components of the two-polarizer apparatus. The apparatus consists of a laser diode, two polarizers, one of which is exporting data to LabView, and a diode detector.

Once a sufficient amount of data was collected for two polarizers, a third polarizer was added behind the acquisition lens, which was then removed to calibrate the second polarizer. This was done by adjusting the second polarizer so that its direction was orthogonal to that of the first polarizer, and a minimal amount of light was being detected in LabView. The acquisition polarizer was then re-added, and LabView was set to record 2π radians as the center polarizer was manually adjusted. Again, this ex-

periment was repeated until the observed data was consistent, uniform, and smooth. The apparatus is depicted in Figure 3:

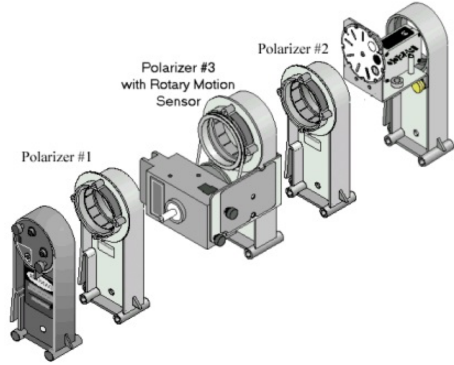


[Figure 3] Depiction of the experimental setup used in verifying Malus's law for three polarizers. The apparatus consists of three polarizers, one of which exports angle data to LabView, a laser diode, and detector.

The last set of trials which were performed were to determine Brewster's angle. The laser detector gain was configured to '10' and a collimating slit was placed in front to avoid over saturating the detector. The detector was attached to a long, rotatable arm. In the center of the rotator was an acrylic D-lens, which angle information was read by an acquisition device and exported to LabView. Incident to the D-lens was diode-laser light which had been polarized and run through a collimating slit to control the amount of light let through. The initial polarizer was the control, and was left in the horizontally-polarized position which was determined from the trials on Malus's law. The experimental apparatus is shown in Figure 4.

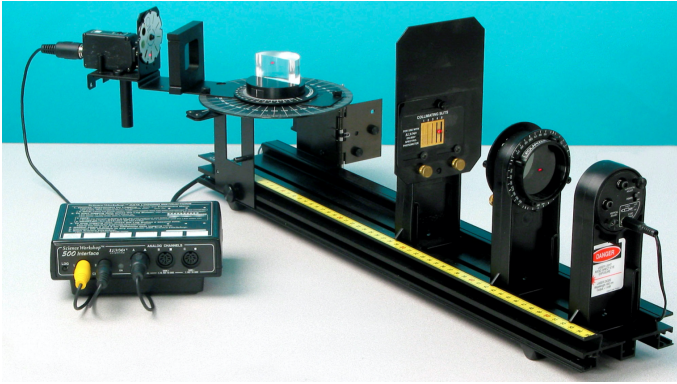


[Figure 4] Experimental setup for determining Brewster's angle. The apparatus consists of a rotatable D-lens, a laser diode, a polarizer, collimating slits and a detector.

Data Analysis

Following the form of the report, Malus's Law will be discussed first. The data, as recorded in *Labview*, was stored in separate .txt files for each of the two trials (2 and 3 polaroids). These files were read by the python library *numpy*'s *readtxt()* function, and isolated by column for *Intensity (V)* and *position (radians)*. The raw data was plotted using another python library, *matplotlib*, with uncertainties (see the upper charts of Figure N and Figure N+1 for the plots of the 2- and 3-polaroid trials respectively). The uncertainties for each of these charts was one half of the smallest significant digit. The plot for 2-polaroids was fit using an equation in the form of (6), and for 3-polaroids was fit using an equation in the form of (7) using *scipy.optimize.curve_fit()*. Each of these functions had additional parameters for a phase-shift and an intensity offset.

The function fit the 3-polaroid trial quite easily, but the 2-polaroid trial was a little bit more tricky. The flatter tails at either end of the sinusoidal wave were culled from the dataset, and the function was able to fit (see Figure N to see the comparison between the original and culled data).

The results of these fits are discussed in the *Results and Discussion section below*. The uncertainties of the relevant parameters of these fits (for these functions, I_0 and I_1 for the 2- and 3-polaroid trials respectively) were found by taking the square root of the covariance of the optimized parameters found by *scipy.optimize.curve_fit*. So long as the maximum value of the curve generated by these optimized pa-

rameters (as well as the majority of the curve itself) fit within the uncertainties of the measured data, the parameters are sufficient, within the uncertainty of the measurements. The residual plots of each trial (the difference between the fit curve and the measured data) were also plotted (the residual plots can be found in the lower charts of Figure N and Figure N+1).

For Brewster's angle, the raw data was imported and plotted in the same way as for the Malus's law experiments (with uncertainties also found in the similar way), but, of course, the angles represent different things, as discussed in the Methodology section (the plots can be found in Figure N+2). These plots have some serious uncertainties in them. The drops in the decay curve are due to the imperfect following of the detector as the reflected light traversed. The large emission area on the horizontally polarized graph (the middle plot in Figure N+2) has some other significant error due to background radiation (a door being opened). But, since only θ_p needs to be extracted from these graphs, none of these errors meaningfully affect the analysis. θ_p was extracted by observing where the horizontally polarized intensity became effectively zero. Using the uncertainty as one half of the last significant digit would be unreasonable in this case since the sampling rate is not perfect, so the uncertainty in this angle was set as $\pm 0.5^\circ$. Equation N was then applied, with $n_1 = 1$ to find n_2 . Equation N+1 was then applied to our now known values to find θ_2 . Now with $n_1, n_2, \theta_1, \theta_2$, everything needed to calculate r_\perp and r_\parallel is known. r_\perp is found using equation N+2 and the sum-of-squares relation (equation N+3) is used to find r_\parallel . For all of these calculations, the uncertainty was propagated using the *uncertainties* python library.

Results and Discussion

For Malus's law, the model found $I_0 = 3.42 \pm 0.01$ V and a phase shift of -0.985 ± 0.003 radians with a $\chi^2 = 0.376$ for the 2-polaroid trial. For the 3-polaroid trial the model found $I_1 = 0.497 \pm 6.8 \cdot 10^{-4}$ V and a phase shift of $1.16 \pm 7.3 \cdot 10^{-4}$ with a $\chi^2 = 0.426$. It is important to notice that, with three polarizers, the intensity is at its maximum when $\varphi = \pi/4$ and at a minimum when $\varphi = 0, \pi$. This might be hard to notice from the graph, but when considering the phase shifts in mind, these values align well with the peaks and troughs of the graphs in Figure 6. Another

important and interesting thing about these results, is that while we managed to find a good fit, there is some strange behavior in the plot of Intensity vs. $\cos^2 \theta$ (figure 7). This graph is expected to be linear, but actually has this strange wing-like shape (see Figure 7). This is surprising since Intensity should be linearly related to $\cos^2 \theta$, but is not.

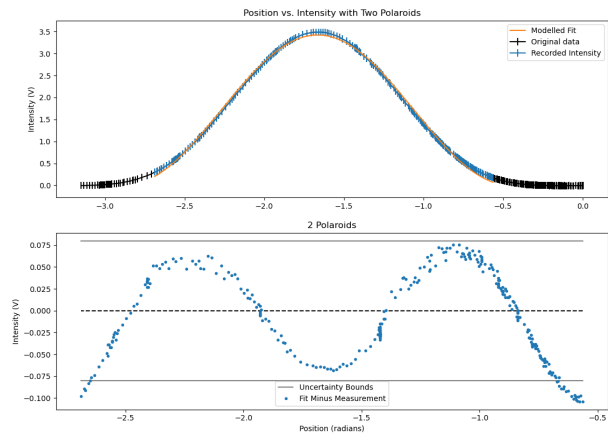
Conclusions

Overall, it was concluded that the thermal diffusivity of the rubber tube was within the range of the expected experimental value specified in literature for polypropylene. Despite difficulties such as tedious data collection, curve fitting, and uncertainty analysis, the results yielded were valid within the uncertainty range.

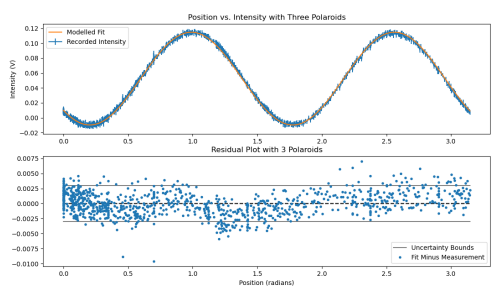
BIBLIOGRAPHY

- [1] Martínez, K., Marín, E., Glorieux, C., Lara-Bernal, A., Calderón, A., Rodríguez, G. P., & Ivanov, R. (2015). Thermal diffusivity measurements in solids by photothermal infrared radiometry: Influence of convection–radiation heat losses. International Journal of Thermal Sciences, 98, 202-207. <https://doi.org/10.1016/j.ijthermalsci.2015.07.019>
- [2] Edge, E. (n.d.). Thermal diffusivity table. Engineers Edge - Engineering, Design and Manufacturing Solutions. Retrieved February 9, 2023, from https://www.engineersedge.com/heat_transfer/thermal_diffusivity_table_13953.htm
- [3] Thermal Diffusivity of Tortured Rubber and Bessel Functions. University of Toronto Practicals, PHY324 Manual. https://www.physics.utoronto.ca/~phy224_324/experiments/thermal-diffusivity/labheat.pdf

Appendix I: Figures and Tables



1: add later.



2: add later.

Trial	Period (s)
$m_1 L_1 \theta_1$	1.442 ± 0.612
$m_1 L_1 \theta_2$	1.623 ± 0.649
$m_1 L_2 \theta_1$	1.275 ± 0.48
$m_1 L_2 \theta_2$	1.11 ± 0.223
$m_2 L_1 \theta_1$	1.386 ± 0.644
$m_2 L_1 \theta_2$	1.434 ± 0.324
$m_2 L_2 \theta_1$	1.181 ± 0.293
$m_2 L_2 \theta_2$	1.369 ± 0.589

[Table 1] Results obtained for the computed values of the thermal diffusivity for each of the three trials. Included is the applied angular period, the intial temperature of the rubber, the curve_fit computed value for the thermal diffusivity and uncertainty, and the quality of the χ^2 fit.

Trial	τ (s^{-1})	χ^2 (probability)
$m_1 L_2 \theta_1$	166 ± 2.1	0.2
$m_1 L_2 \theta_2$	334 ± 12	0.3
$m_1 L_2 \theta_1$	86.5 ± 49	0.0
$m_2 L_2 \theta_1$	26.9 ± 6.9	0.0

[Table 1] Results obtained for the computed values of the thermal diffusivity for each of the three trials. Included is the applied angular period, the intial temperature of the rubber, the curve_fit computed value for the thermal diffusivity and uncertainty, and the quality of the χ^2 fit.